# Chapter 7

# Travel time tomography of western North America with a new arrival time data set

## 7.1 Introduction

The west coast of North America has been, and still continues to be, a site of complex deformation due to its location near a major plate boundary. In Mesozoic and Cenozoic times, the Farallon plate (an oceanic plate west of the North American plate) was subducted eastward under the North American plate. In the Cenozoic (29 Ma ago), subduction of the Farallon plate beneath southern California was completed while subduction of the remaining northern part, called Juan de Fuca and Gorda plate (see Fig. 7.1), continued. With cessation of subduction in the south a transform fault between the northwestward moving Pacific plate and the westward moving North American plate was created (plate motions relative to Africa) and the Mendocino Triple Junction between Pacific, Juan de Fuca and North American plate formed. This triple junction started moving northward 25 Ma ago and was accompanied by an extinction of the arc volcanism along its way and initiation of volcanism in the northern Coast Range.

Tomography provides information which helps to reconstruct tectonic movements in that region. On a long-wavelength scale, surface wave tomography models exist, which image the upper mantle beneath the North American continent (e.g. van der Lee and Nolet, 1997; Godey *et al.*, 2003). However, in higher detail mostly local or regional models exist which do not image the entire region. For example, the subduction beneath the Cascades of Washington and Oregon was imaged by Michaelson and Weaver (1986), Rasmussen and Humphreys (1988) and Neele *et al.* (1993) and it was subject of the Cascadia 1993 experiment carried out across central Oregon to image the subduction of the Juan de Fuca plate under the North American plate. As part of this experiment, Rondenay *et al.* (2001) and Bostock *et al.* (2002) obtained a high-resolution image of the upper 120 km of the subduction zone. The Gorda slab and its

southern edge have been imaged by Benz *et al.* (1992) and Beaudoin *et al.* (1998) among other studies. The uppermost mantle beneath the southern Great Valley and the Sierra Nevada has been investigated by many authors with receiver functions, regional tomography and shear wave splitting (e.g. Benz and Zandt, 1993; Boyd *et al.*, 2004; Zandt *et al.*, 2004; Yang and Forsyth, 2006). In particular, many more crustal studies exist of northwestern America but as we focus on the mantle they will not be listed here.
In contrast to these local or regional studies, we will present here a comprehensive high-resolution tomography model of northwestern America based on new data combined with ISC (International Seismological Centre) and NEIC (National Earthquake Data Center) bulletin data.

## 7.2 Data

### 7.2.1 Newly picked data for stations in North America

For many recordings of the Advanced National Seismic Network (ANSS), the Incorporated Research Institutions for Seismology (IRIS), Canadian National Seismic Network (CNSN), Southern California Earthquake Data Center (SCEDC) and the NARS-Baja project arrival times were not determined and therefore not reported to the ISC. These recordings build the basis of the new, additional data set used here. Seismograms from these stations were obtained, pre-processed and picked by Sandoval *et al.* (2004a) with an automatic picking method to investigate the lithosphere and mantle beneath North America but so far, the data set has not been used for tomography. The data from that project were recorded from 2002–2004 and contain 120,000 P-wave picks for 486 events (event and station locations are given in Fig. 7.1).

### 7.2.2 EHB catalog

The main data source for travel time tomography in this study is a reprocessed and updated version of the International Seismological Centre (ISC) bulletins extended with travel times from the National Earthquake Information Center (NEIC) of the USGS for the most recent events by Engdahl *et al.* (1998). This database will be referred to hereafter as EHB catalog. It contains earthquake observations for the period 1964–2004 including over 445,000 events for 27.4 million first and later arriving phases. The processing of Engdahl *et al.* (1998) comprised a phase re-identification, theoretical travel time calculation in the Earth reference model ak135 (Kennett *et al.*, 1995) and a relocation of the events. From this data set, 19.1 mill. arrival times (P, pP, pwP, PcP, PKP and PKiKP phases) were selected for tomography.

## 7.3 Method

The method applied here is travel time tomography, which uses the difference between observed and predicted arrival times of P-waves to compute velocity variations within the investigated region with respect to a reference model. The theoretical arrival times are also

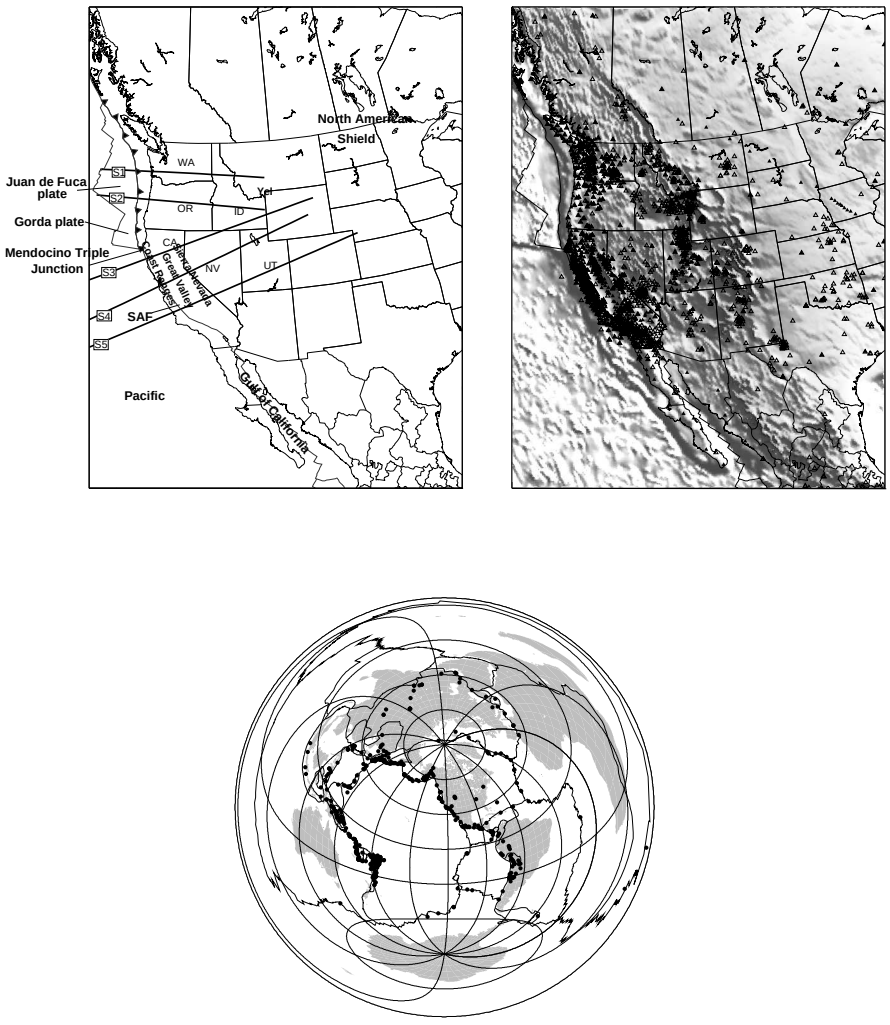


**Figure 7.1:** The lines S1-S5 on the top left give the location of model cross sections displayed later on (Fig. 7.4). Abbreviations: SAF – San Andreas fault, Yel – Yellowstone. In the map on the upper right, open triangles indicate the location of stations contained in the EHB catalog. Filled triangles show station locations of additional data. Illustrated in the bottom figure are the locations of the earthquakes contained in the new arrival time data set.

calculated with this reference velocity model, which is here the 1-D model ak135 by Kennett *et al.* (1995) and additionally for a later inversion a 3-D reference model. This 3-D reference model contains the global travel time tomography model obtained with respect to ak135 in regions of good ray coverage. The anomalies of the model are amplified up to a factor of 2 where allowed by the model null space as anomaly amplitudes are usually underestimated in travel time tomography in many mantle regions by 30%-50%. Otherwise, CUB2.0 (Ritzwoller *et al.*, 2002a), which is based on CRUST2.0 (Bassin *et al.*, 2000) in the crustal part, is used in the uppermost mantle and below that S20RTS (Ritsema *et al.*, 1999). For usage of the 3-D reference model, the earthquakes are relocated in that model to ensure consistency of source parameters and travel times. For more details on the use of 3-D reference models for travel time tomography see Chapter 5.

We use the method of Bijwaard *et al.* (1998) to solve the inverse problem. Even though focus is on northwestern America, a global tomography experiment is performed thereby avoiding all shortcomings of using a regionally defined model volume. Composite rays are used instead of single rays, where a composite ray is built from single rays of the same phase type which originate from the same event cluster and end at the same station. By using composite rays, the amount of data for inversion is reduced but at the same time the signal-to-noise ratio is increased. The data are weighted prior to inversion by the spread of the individual delay times within the respective ray bundle to account for the difference in ray bundle size. For the new data, this approach is not used as their quality is expected to be higher. Instead, single rays are used. The resulting data vector then contains 10.4 million residuals.

The Earth is parameterized by an irregular grid of non-overlapping cells following the approach of Spakman and Bijwaard (2001) where the cell size depends on the number of rays crossing a cell. The cell size varies in crust and mantle between $0.5° \times 0.5°$ and $10.0° \times 10.0°$ with an increasing layer thickness from the crust (10 km) to the lower mantle (200 km). The core is parameterized by a single layer for each, inner and outer core, with cells of $10° \times 10°$ to account for rays crossing through the core but to suppress strong model variations at the same time. Using such an irregular grid has the advantage of reducing the number of unknowns from 8 035 000 to 604 000, reducing the overparameteratization (and therefore the regularization needed during inversion) and retaining the possibility to resolve structure at small scales where allowed by the data.

The tomographic inversion itself is performed iteratively with the LSQR algorithm of Paige and Saunders (1982). A second-derivative damping is applied to regularize the solution of the inversion and to obtain a smooth model. Additionally, for inversion with 3-D reference models an amplitude damping is applied to suppress large excursions from the reference model.

## 7.4 Model recovery

As stations and events are not equally distributed over the investigated region, the resolution of the velocity model varies spatially. The uneven data distribution is clearly indicated in the hitcount map (Fig. 7.2) which gives the number of rays traversing a cell. For example, ray coverage at shallow depths is low beneath the Pacific due to a lack of earthquakes and stations. Also for the North American shield there is a lower ray coverage due to a low number of events and seismic stations. The new data increase ray coverage mainly along the

western part of the United States, in particular, beneath California and Washington.
As the computation of the resolution matrix is too time consuming due to the large number of parameters, tests are performed with synthetic spike models (e.g. Spakman and Nolet, 1988) of various spike sizes to estimate the resolution. These tests are performed with respect to ak135 and the synthetic models contain spikes of $\pm$ 5% amplitude which are projected onto the irregular grid. Theoretical travel times are then calculated using the ray distribution of the observed data and Gaussian noise with a standard deviation of $\pm 0.5$ s is added to the data. Subsequently, the resulting matrix-vector equation is inverted. The result of spike tests with $0.5^\circ \times 0.5^\circ$, $1.0^\circ \times 1.0^\circ$ and $2.0^\circ \times 2.0^\circ$ spikes is displayed in Figure 7.2 at 50 km and 440 km depth. Spike anomalies are recovered in the western part of the United States where ray coverage is high with a minimum size of reconstructable spikes between at $0.5^\circ \times 0.5^\circ$ in the uppermost mantle and $3.0^\circ \times 3.0^\circ$ in the lower mantle (not shown).

## 7.5 Results

The tomography results are displayed in Figure 7.3 for inversion of the new data combined with the EHB data using ak135 as reference model (P06) and using a 3-D reference model (P06_3Dloc). To get a better impression of these models, they are compared to the model "BSE" of Bijwaard *et al.* (1998) which was obtained with a smaller data set but using the same method as here and applying ak135 as reference model. Consequently, P06 bears many similarities with BSE. Even though different reference models are used in the inversions, all models are displayed with respect to ak135 for comparison.
At 50 km depth, in model P06 the North American shield is imaged by high velocities. Beneath most of California except for the southernmost part, the San Andreas fault is resolved as boundary between the high velocities of the Pacific plate and the low velocities of the North American plate. The new data sharpen the velocity contrast between the Pacific and North American plate south of San Francisco. Furthermore, a comparison with the BSE model shows that the model is better resolved now with smaller grid cells beneath the North American shield as the latest EHB data set contains significantly more regional data. Differences in the tomography model using a 3-D reference model (P06_3Dloc) compared to P06 appear, in particular, where the ray coverage with short period P-waves is low and therefore mainly the 3-D reference model is re-obtained as beneath the Pacific or parts of the craton where low instead of high velocities are imaged as this region, at 50 km depth, is partly considered as crust in the reference model. Otherwise, anomaly amplitudes are mainly strengthened compared to P06.
At 185 km depth, the additional information of the new data is already reduced being still highest along the coastline. As main features in P06, a high-velocity anomaly parallel to the coastline could be imaged and low velocities beneath Yellowstone. The new data enhance the northern part of the high-velocity anomaly beneath Washington while in the south, the amplitudes of these anomalies are left unchanged but compared to the BSE model in the central part the velocities are decreased. Also, along the Gulf of California ridge, velocities are further decreased due to the new data. In the eastern half of the cross section other differences between BSE and P06 are found resulting in a better outlined boundary of the high-velocity anomaly in P06 beneath the shield towards the west. Usage of the 3-D reference

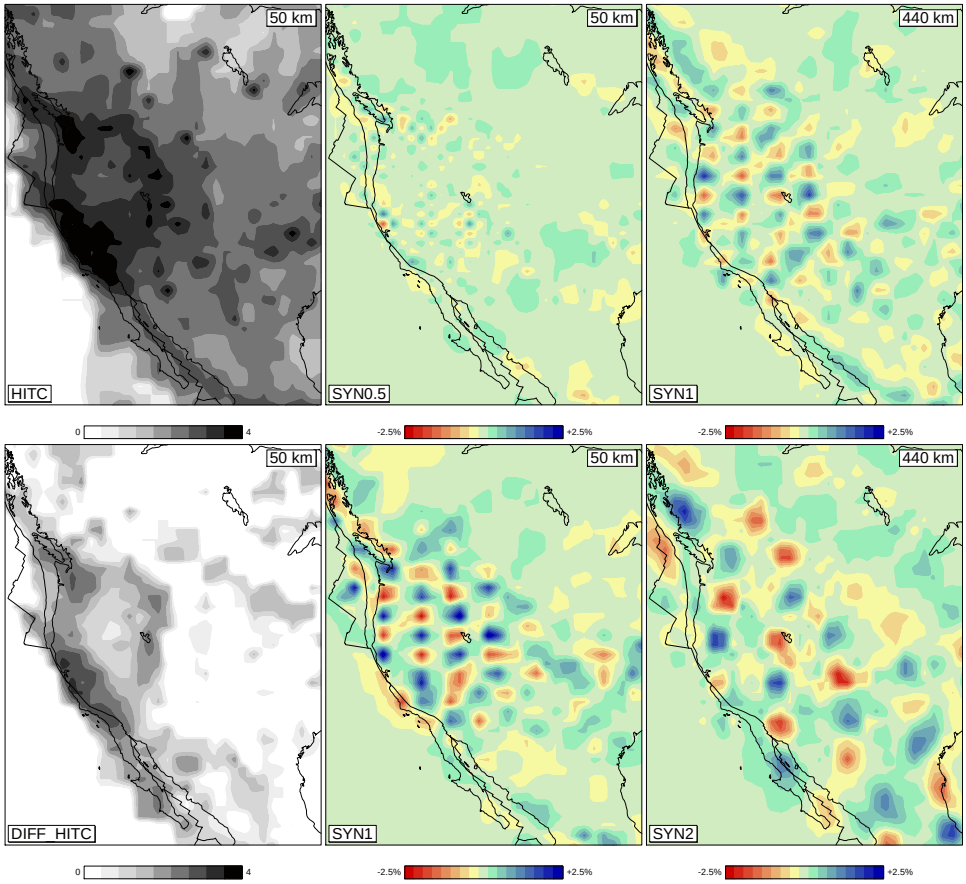


**Figure 7.2:** Displayed at 50 km depth is the hitcount of the combined data set (left, top), the addition of the new data to the hitcount (left, bottom), a $0.5^\circ \times 0.5^\circ$ and $1.0^\circ \times 1.0^\circ$ spike test using the combined data set (middle, top and bottom) and at 440 km depth a $1.0^\circ \times 1.0^\circ$ and $2.0^\circ \times 2.0^\circ$ spike test using the combined data set (right, top and bottom).

model provides again implicitly more realistic velocities beneath the Pacific and below the cratonic part of North America thereby enhancing the contrast to the tectonically active region of the North American Cordillera.
At 440 km depth in the upper mantle transition zone, P06 is dominated by low velocities beneath northwestern America but contains high velocities beneath Nevada, Utah and Idaho. Also, at this depth the signature of the North American shield has vanished and is replaced by a low-velocity anomaly. Differences with BSE are biggest in the eastern half of the section where P06 contains more data and therefore gives a more coherent image. The model using a 3-D reference/starting model is comparable to the model using a 1-D reference/starting model except for the Pacific where P06_3Dloc contains the low velocities of S20RTS.
To get a better impression of the distribution of high-velocity anomalies and their interchange with low-velocity anomalies, vertical cross sections through the models presented in Figure 7.3, are displayed in Figure 7.4. The exact location of the slices is given in Figure 7.1. Starting in the northern part of the model with a west-east trending slice (S1), the aforementioned high-velocity anomaly represents the subducted Juan de Fuca slab beneath North America. This slab is steep in the western part and flattens in the upper mantle transition zone. The new travel time residuals increase velocities particulary in the uppermost and lowermost section of the slab. The BSE model contains also above the 410 km discontinuity smeared out high velocities related to a lack of data.
Further south (S2), the slab is only observed with high velocities down to approximately 200 km depth with resolution being sufficient to reconstruct anomalies at this depth. The new data amplify the surrounding low velocites and compared to BSE, the high-velocity anomaly is more focussed.
Further south (S3), in P06 and P06_3Dloc the Gorda slab becomes again a more continuous feature lying flat in the top part of the transition zone. Compared to BSE the new data in combination with the latest EHB data set clearly improve the amplitudes of the slab anomaly. In the next slice further south (S4), a high-velocity anomaly cannot be found where it was seen before in the uppermost mantle while below 350 km depth it is detected. Again, the high-velocity anomaly in P06 and P06_3Dloc is more focused than in the BSE model.
Even further south (S5), this anomaly in the transition zone is observed again with weaker amplitudes. However, in the uppermost mantle a high-velocity anomaly east of the San Andreas fault is found in all models and the new data increase the velocities of that anomaly. Due to the different reference model, the connection of the high-velocity drip disappears in the model using a 3-D reference (P06_3Dloc).

## 7.6 Discussion and Conclusions

The new data clearly improve the tomographic model in the uppermost mantle and in regions that were sparsely sampled in previous global tomography studies (e.g. Bijwaard *et al.*, 1998). A subducted slab can be detected in the uppermost mantle from British Columbia to approximately 170 km south of the Mendocino triple junction and vanishing/weakening below $\sim 200$ km depth beneath Oregon close to the boundary between Juan de Fuca and Gorda plate.
Earliest indicators of a high-velocity slab beneath southwestern Canada and the northwestern

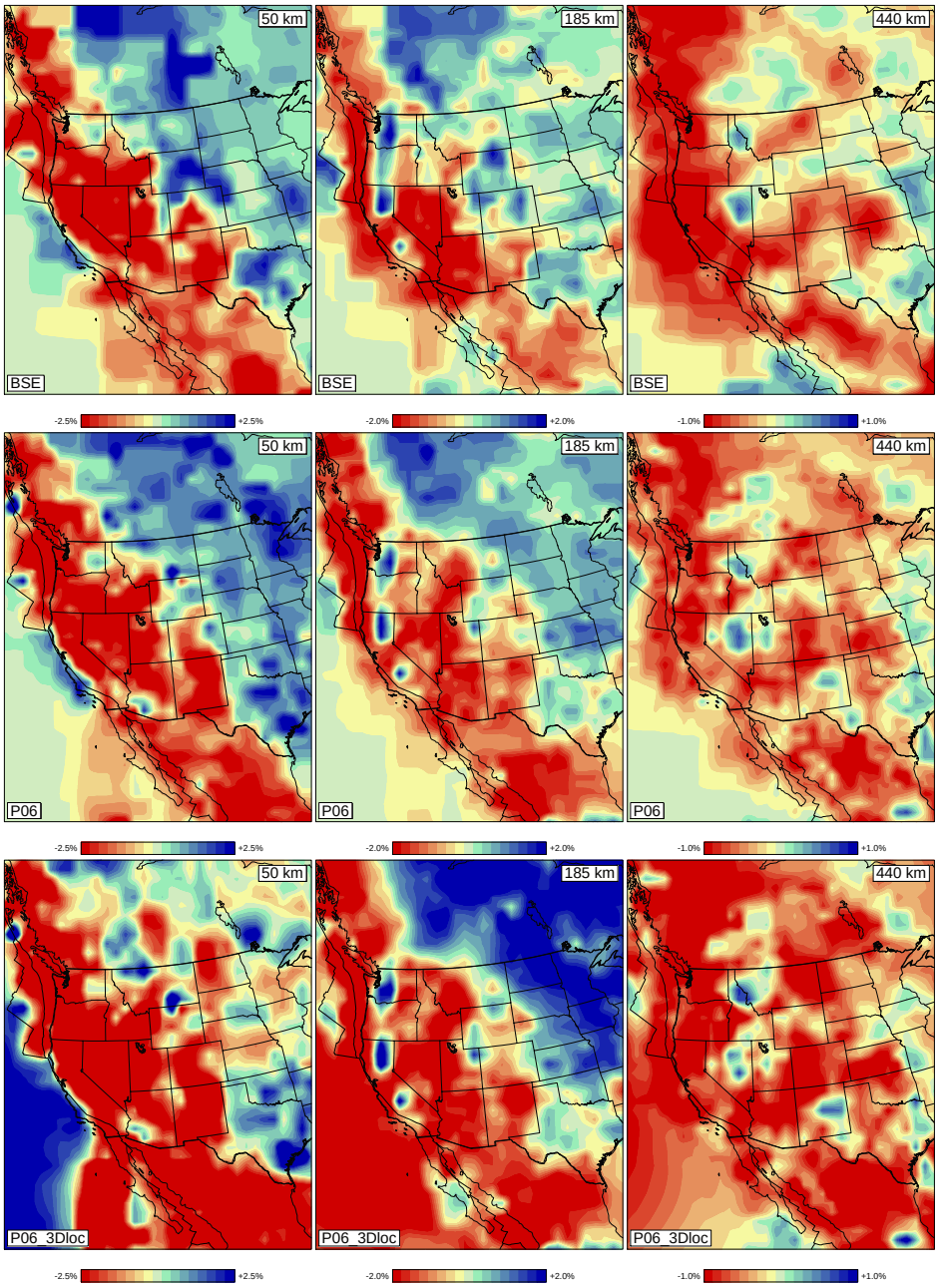


**Figure 7.3:** The BSE model of Bijwaard *et al.* (1998) (top row), the model using the newly picked data and EHB data with a 1-D reference model (middle row) and the model using the new data and EHB data with a 3-D reference model (bottom row) at 50 km (left), 185 km (middle) and 440 km depth (right). All velocity perturbations are displayed with respect to ak135 independent of the starting model used for tomographic inversion.

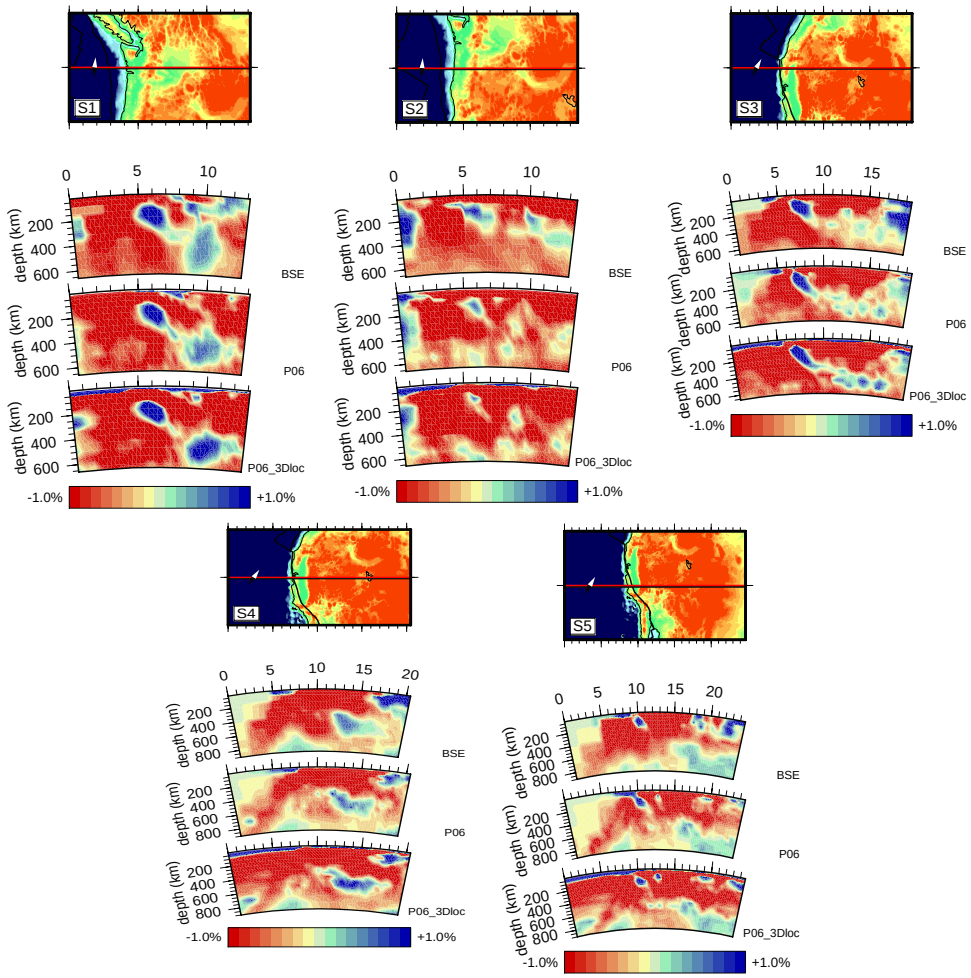


**Figure 7.4:** Vertical cross sections through the models as displayed in Fig. 7.3. The location of the cross sections is displayed in Fig.7.1. The velocity perturbations are given with respect to ak135 .

United States were observations of P travel times (McKenzie and Julian, 1971). The part of the slab beneath Oregon and Washington was also detected in an inversion of teleseismic P travel times by Michaelson and Weaver (1986), Rasmussen and Humphreys (1988) and VanDecar (1991). The model of Rasmussen and Humphreys (1988) extends furthest south with a similar depth extent of the high-velocity to our model to at least 400 km in the northern part of their model (corresponding to S1) and 200 km in the southern part (corresponding to S2). However, our model continues further to the east and we are therefore able to image the flattening of the slab below 400 km depth.
The part of the Gorda slab (S3) beneath California was imaged earlier by Benz *et al.* (1992) with teleseismic P tomography. Its southern edge of the Gorda plate has been imaged by Beaudoin *et al.* (1998) with a seismic refraction-reflection profile being located at approximately $40°$N beneath California, which is in good agreement with our model where the slab at 200 km depth extends to approximately $39°$N.
The low-velocity region at the southern end of the Gorda slab (S4) and the adjacent high-velocity anomaly beneath Central California (S5) have been subject of debate for many years. Ten Brink *et al.* (1999) suggest that the low-velocity anomaly (S4) represents a region of stretched slab material where thermal re-equilibration causes the observed low-velocity anomaly. As another possibility, Furlong *et al.* (1989), Benz *et al.* (1992) and Benz and Zandt (1993) interpret the low-velocity region as a slab window in which asthenospheric material is upwelling. According to our model, the low-velocity anomaly beneath Central California is caused by hot upwelling asthenosphere material that moved in after subduction ended and the slab sank into the mantle since remnants of this slab are still observable further to the east from 350 km depth onwards. Benz and Zandt (1993) suggest that the high-velocity anomaly at the southern end of the slab window below the southern Great Valley (S5) is caused by a fragment of the Farallon plate being left there after subduction ended. Zandt and Carrigan (1993) also interpret the slab window as a region where upwelling asthenosphere replaced the remnants of the Farallon slab after cessation of subduction in southern California. However, they interpret the high-velocity anomaly south of the slab window as a body dripping off the base of the lithosphere due to a small-scale convective instability. This theory was later on supported by a time-dependent simulation of the thermal evolution of the asthenosphere (Liu and Zandt, 1996) and Ruppert *et al.* (1998) and Saleeby *et al.* (2003) proposed the southern Sierra Nevada batholitic root as origin of the detached lithosphere. Also Zandt *et al.* (2004) come to the conclusion that this high-velocity anomaly represents either the root of the southern Sierra Nevada or a downwelling induced by foundering of the root. A recent seismic tomography study of the lithosphere beneath the southern Sierra Nevada with P and S wave travel times (Boyd *et al.*, 2004) confirms the existence of the high-velocity drip but dipping eastward beneath the southern Sierra Nevada. Boyd *et al.* (2004) conclude from analyses regarding composition and temperature that the anomaly represents stratified mantle lithosphere delaminated from the crust beneath the southern Sierra Nevada.
Our model does not allow for inferences on compositional and thermal aspects of the anomaly but unlike previous regional tomography studies, we are able to give a depth limit for the high-velocity anomaly confining it to a depth $< 250$ km. The obtained model agrees well with other studies that prefer removal of the Sierra Nevada root as cause of the high-velocity anomaly (instead of a Farallon slab fragment) and we observe the remnants of the Farallon

slab above the 660 km discontinuity further east of the high-velocity anomaly. Therefore, the most plausible explanation for the eastward dipping high-velocity anomaly below the southern Great Valley and Sierra Nevada is a drip of lithospheric root from the southern Sierra Nevada.
In summary, we have been able to image the P velocity structure beneath entire northwestern America in high detail with global travel time tomography. Newly picked arrival times have, in particular, improved the model in the uppermost mantle in region where ray density was low before thereby enhancing, for example, the outlines of subducted slabs.

## 7.7 Acknowledgments

We thank the ISC, NEIC, ANSS, CNSN, IRIS, SCEDC and NARS-Baja working group for providing the data used in this study and M. Ritzwoller and J. Ritsema for providing the 3-D reference models used in this study. Computational resources for this work were provided by the EUROMARGINS programme of the European Science Foundation (01-LEC-MA22F WESTMED) and by the Netherlands Research Center for Integrated Solid Earth Science (ISES 3.2.5 High End Scientific Computation Resources).

# Chapter 8

# Relocation of a global earthquake data set with a 3-D velocity model

We have relocated a global earthquake data set of 450,000 events contained in the International Seismological Centre (ISC), National Earthquake Information Center (NEIC), Europe-Mediterranean Seismological Centre (EMSC) and regional network data bases. The initial earthquake locations were obtained using a standard 1-D Earth reference model while the earthquake relocations presented in this study were performed in a highly detailed 3-D velocity model based on travel time tomography using a directed grid search technique. Tests with well-located events show an improvement of the earthquake location errors using the 3-D model with respect to a 1-D Earth reference model. Furthermore, systematic source parameter shifts of the events in the global earthquake data set can be observed with respect to their initial location which are caused by 3-D Earth structure now accounted for in the earthquake location process.

## 8.1 Introduction

Accurate earthquake locations are important not only for seismo-tectonic and seismic hazard assessment but also for the Comprehensive Nuclear Test-Ban Treaty (CTBT) or for tomography studies investigating the velocity structure of the Earth's crust and mantle. The accuracy of event locations depends on many factors among which are the number of phases used for computation of the location, proper phase identification, the velocity model used for computation of reference travel times and the location method itself. Besides the ISC and NEIC, which provide global data sets of earthquake locations, the updated EHB catalog of Engdahl *et al.* (1998) provides a groomed version of the ISC and NEIC bulletins from 1964 to 2004 including improvements compared to other global catalogs. The earthquake locations in the EHB catalog were obtained using a 1-D Earth reference model adding regionally averaged travel time corrections for upper mantle structure. Furthermore, phase identification of depth phases in this catalog was improved using probability density functions of later-arriving phases. The 3-D velocity heterogeneities in the source regions and along the ray paths of the